




## Article

# An Automated Approach for Calibrating Gafchromic EBT3 Films and Mapping 3D Doses in HDR Brachytherapy

Labinot Kastrati <sup>1,2</sup>, Burim Uka <sup>2,3,4</sup> , Polikron Dhoqina <sup>4</sup>, Gezim Hodolli <sup>5,\*</sup> , Sehad Kadiri <sup>2,6</sup>, Behar Raci <sup>2</sup>, Faton Sermahaj <sup>2</sup>, Kjani Guri <sup>3</sup>  and Hekuran Sejdiu <sup>2</sup>

<sup>1</sup> Faculty of Mechanical and Computer Engineering, University of Mitrovica “Isa Boletini”, 40000 Mitrovica, Kosovo; labinot.kastrati@umib.net

<sup>2</sup> Clinical Oncology, University Clinical Center of Kosovo, 10000 Prishtina, Kosovo

<sup>3</sup> Faculty of Medical Sciences, University for Business and Technology, 10000 Prishtina, Kosovo

<sup>4</sup> Faculty of Natural Sciences, University of Tirana, 1000 Tirana, Albania

<sup>5</sup> Faculty of Veterinary and Agriculture, University of Prishtina, 10000 Prishtina, Kosovo

<sup>6</sup> Faculty of Radiology, AAB College, 10000 Prishtina, Kosovo

\* Correspondence: gezim.hodolli@uni-pr.edu

## Abstract

The accurate calibration of radiochromic films is critical for high dose rate (HDR) brachytherapy dosimetry. Conventional workflows frequently rely on manually determined regions of interest (ROIs), which might increase operator variability. In this investigation, Gafchromic EBT3 films were irradiated under clinical settings at nominal doses of 0–10 Gy and evaluated using a MATLAB (R2024b)-based tool that allows for both manual and automated ROI selection. The calibration curves were modeled with a second-order polynomial and rational model, and performance was assessed using statistical measures. The study found that the rational model fits better than the polynomial model. Additionally, the automatic ROI approach outperformed the manual method in both models, resulting in higher calibration accuracy and reproducibility ( $R^2 = 0.999$ , RMSE = 0.118 Gy, MAE = 0.103 Gy vs.  $R^2 = 0.986$ , RMSE = 0.448 Gy, MAE = 0.388 Gy). Although manual ROI occasionally produced greater dose–response slopes at higher doses, it was more susceptible to operator bias and film non-uniformity. In contrast, automatic ROI reduced variability by consistently picking homogeneous sections, resulting in steady curve fitting across the entire dose range. Furthermore, a companion module transformed calibrated films into 2D false-color maps and 3D dosage surfaces, allowing for visual assessment of dose uniformity, detection of scanner-related aberrations, and quantitative verification for quality assurance. These findings demonstrate that automated ROI selection provides a more stable and reproducible foundation for film calibration in HDR brachytherapy, minimizing operator dependency while facilitating routine clinical quality assurance.

**Keywords:** Gafchromic; EBT3; brachytherapy; calibration curve; absorbed dose



Academic Editor: Chang Ming Charlie Ma

Received: 5 September 2025

Revised: 2 October 2025

Accepted: 4 October 2025

Published: 9 October 2025

**Citation:** Kastrati, L.; Uka, B.; Dhoqina, P.; Hodolli, G.; Kadiri, S.; Raci, B.; Sermahaj, F.; Guri, K.; Sejdiu, H. An Automated Approach for Calibrating Gafchromic EBT3 Films and Mapping 3D Doses in HDR Brachytherapy. *Appl. Sci.* **2025**, *15*, 10833. <https://doi.org/10.3390/app151910833>

**Copyright:** © 2025 by the authors. Licensee MDPI, Basel, Switzerland. This article is an open access article distributed under the terms and conditions of the Creative Commons Attribution (CC BY) license (<https://creativecommons.org/licenses/by/4.0/>).

## 1. Introduction

Brachytherapy is a key method in modern radiation oncology, providing highly localized dose administration that protects healthy tissues while delivering excellent tumor control [1,2]. It is commonly used in the treatment of gynecological, prostate, breast, and other cancers, where its precision and conformality allow for both curative and palliative outcomes. Brachytherapy’s capacity to deliver high doses in a short treatment period makes it not only clinically beneficial but also cost-effective, cementing its place as a standard of

care in many cancer treatment regimens. Brachytherapy creates a very steep dose gradient with rapid fall-off near the source, while linear medical accelerator external beam therapy has a shallow gradient shaped by beam modulation [3].

The proper estimation of absorbed dose is one of the most important parts of brachytherapy, since even small errors can have a direct impact on tumor control and normal tissue complication probability. Precise dosimetry ensures that recommended doses match delivered doses, protecting both therapy efficacy and patient safety [1]. Inaccurate dose assessment might result in either underdosage (tumor recurrence) or overdosage (severe toxicity in surrounding healthy tissues).

Several detection technologies are currently being used in clinical and research settings to accomplish high-accuracy dose verification. Because of their small size and tissue equivalence, thermoluminescent dosimeters (TLDs) [4] are still commonly employed, but with careful annealing and readout methods. Optically stimulated luminescence dosimeters (OSLDs) [5] are desirable for postal audit programs due to their re-readability and increased sensitivity. Ionization chambers are still the gold standard for reference dosimetry [6], providing traceable and very accurate dose measurements; however, their limited spatial resolution limits their use in steep dosage gradients typical of brachytherapy. Semiconductor diodes and plastic scintillators are also used in some situations to provide near-real-time measurements with high sensitivity. More recently, radiochromic films such as Gafchromic EBT3 [7] have gained popularity because of their excellent spatial resolution, near tissue equivalence, and capacity to generate two- and three-dimensional dose distributions, all of which are extremely useful in HDR brachytherapy quality assurance.

Accurate dose administration in high-dose-rate (HDR) brachytherapy is critical for enhancing therapeutic efficacy while limiting harm to nearby healthy tissues. Radiochromic films, specifically Gafchromic EBT3, have proven themselves as valuable instruments in dosimetric verification because of their excellent spatial resolution, near tissue equivalence, and self-developing features [8]. These films avoid the requirement for chemical processing and give a consistent, quantitative estimate of optical density that is proportional to absorbed radiation exposure. In this investigation, we use commissioned clinical-grade equipment to irradiate Gafchromic films and generate exact calibration curves. These curves allow for reliable evaluation of dose distributions provided to patients during brachytherapy treatments. The calibration performs several key functions, including verifying real dose distribution during treatment, documenting dose delivery for quality assurance, and evaluating new or aged applicators to detect potential manufacturing faults or performance decline over time.

Recent studies have verified the use of Gafchromic EBT3 films to assess the dosimetric properties of Ir-192 sources. Calibration-based evaluations of dose rate constants, radial dose functions, and anisotropy functions for a 192 Ir Flexisource showed variances below clinically acceptable limits ( $\leq 5\%$ ) when compared to published reference data [8,9]. Calibration of EBT3 films with an Ir-192 source is feasible and reliable. However, calibration with 6 MV photon beams may result in dose-dependent accuracy [10]. Furthermore, advanced calibration techniques are evolving. A recent discovery comprises a novel surface brachytherapy mold tested with Gafchromic EBT3 films and Monte Carlo simulations, emphasizing the applicability of film dosimetry for quality assurance of custom applicator designs [11]. Additionally, postal dosimetric audits using radiochromic films have been proposed for HDR brachytherapy with Ir-192 and Co-60 sources, demonstrating the significance of film dosimetry within institutional quality control frameworks [12].

Innovative dosimetric approaches are also emerging. Raman micro-spectroscopy enables high-resolution calibration of EBT3 films over a wide dosage range (0.03–50 Gy), resulting in sub-millimeter dose mapping with uncertainty analysis [13]. Radiochromic

films are also being used in cutting-edge applications, such as very-high-energy electron (VHEE) and ultra-high dose-rate (UHDR) FLASH therapy, where optimized RCF protocols achieved dose agreement within 5% compared to alanine dosimeters [14].

Despite the availability of numerous dosimetric techniques, radiochromic film calibration in the literature often relies on manually selected regions of interest (ROIs). This manual procedure introduces subjectivity and variability among operators because the film portions chosen may contain scanner non-uniformities, edge artifacts, or handling marks. As a result, the reliability of calibration curves can be jeopardized, and systematic inaccuracies can spread to dosage verification results. Currently, there is a significant shortage of automated approaches for ROI selection in film dosimetry that could provide objective, reproducible, and error-minimized calibration curves for clinical quality assurance in brachytherapy.

The Gafchromic EBT3 films were exposed to clinical irradiation conditions, and a calibration technique was developed to increase the accuracy and reproducibility of film-based dosimetric measurements. Unlike most published research, which involves manually selecting regions of interest (ROIs), we created a MATLAB-based system that enables both automated ROI detection and manual ROI selection on the same irradiation film. This dual approach produces calibration curves using two different strategies, allowing for a direct comparison of their accuracy and robustness. The fundamental purpose of this research is to evaluate the reliability of automated ROI selection as an alternative to standard human ROI definition in order to increase calibration consistency and reduce operator-dependent variability.

In the current study, Gafchromic EBT3 films were exposed to clinical irradiation settings, and a calibration technique was developed to increase the accuracy and consistency of film-based dosimetric measurements. Unlike most published research, which involves manually selecting regions of interest (ROIs), we created a MATLAB-based system that enables both automated ROI detection and manual ROI selection on the same irradiated film. This dual technique permits the creation of calibration curves using two distinct strategies, allowing for a direct comparison of their accuracy and robustness. The fundamental purpose of this research is to evaluate the reliability of automated ROI selection as a replacement for traditional human ROI definition in order to increase calibration consistency and reduce operator-dependent variability.

The novelty of this study lies in the development of an automated ROI selection algorithm combined with MATLAB-based 2D/3D dose visualization. Unlike previous works that mainly relied on manual ROI selection, this approach minimizes operator dependence, improves reproducibility, and provides an integrated calibration-to-visualization workflow for HDR brachytherapy quality assurance.

## 2. Materials and Methods

### 2.1. Film Dosimeters Preparation and Vaginal Applicator Setup

Six Gafchromic EBT3 films from the same production LOT 03082201, produced date 8 March 2024, were utilized in this work to maintain batch uniformity and reduce inter-lot variability. Films were handled only using powder-free gloves to avoid contamination, scratches, or bending, which could impair dosimetric accuracy. The films were stored in light-protected envelopes under controlled room temperature ( $20 \pm 1$  °C) and relative humidity (40–60%).

The films were cut into conventional dimensions of  $6.3 \times 12.5$  cm to wrap around the cylindrical vaginal applicator (diameter 40 mm) without overlapping or excess slack. To ensure orientation throughout the procedure, each film piece was labeled with the expected irradiation dose and an orientation arrow. This resulted in consistent alignment during

cutting, irradiation, scanning, and data analysis. To create stable and reproducible contact, the films were wrapped around the applicator with elastic rubber bands, ensuring a tight fit and preventing air gaps (Figure 1).

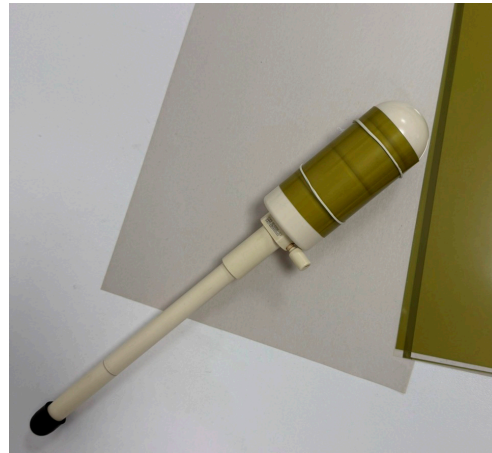


**Figure 1.** Vaginal applicator wrapped with an EBT3 film dosimeter.

Following film preparation, the applicator with the attached film was positioned at the center of a water-equivalent phantom (WP1D Water Phantom, PTW Freiburg, Germany) filled with distilled water (Figure 2).



**Figure 2.** Computer Tomography (CT) simulation of applicator with EBT3 film inside of water phantom.

The use of water as the embedding medium is essential for replicating full-scatter conditions similar to the clinical environment, as water closely approximates soft-tissue equivalence in terms of radiation absorption and scattering. This arrangement ensures that dose distribution measurements obtained from the films accurately reflect the true dosimetric conditions experienced *in vivo*.

The vaginal applicator is gynecological equipment used for brachytherapy treatments. It comprises a vaginal tube, intrauterine tubes with various curvatures (15°, 30°, and 45°),

and interchangeable cylinders with diameters of 20, 25, 30, 35, and 40 mm. The applicator is made of magnetic resonance (MR)-safe composite materials, which eliminate artifacts in CT or MR imaging and allow for conformal treatment planning using transversal slices. Its modular design enables adaptation to various patient anatomies while maintaining optimal dose distribution and consistency during irradiation.

In the current study, the largest available cylinders with a diameter of 40 mm were chosen. The justification for this decision is that increasing the distance between the film dosimeter and the radiation source minimizes the dose gradient, reducing measurement sensitivity to minor positioning mistakes and resulting in smoother, more uniform dosage profiles. This is especially crucial for appropriate calibration since it prevents over-response in areas directly close to the source and ensures that film readings reflect clinically relevant scatter circumstances.

## 2.2. CT Simulation

A CT simulation was performed to simulate clinical irradiation conditions and allow for exact dose calibration in the phantom system. The vaginal applicator, with the calibration tape wrapped around its outer surface, was centrally positioned in a WP1D water phantom (PTW, Freiburg, Germany) filled with distilled water to establish full scatter conditions, as shown in Figure 2. The water was used because it has absorption and dispersion properties similar to human tissue, guaranteeing that the observed dose distribution resembled in vivo circumstances, while the central location reduced boundary effects and provided symmetric scatter for reproducible calibration. Imaging was performed with the Siemens Somatom GoSim simulator, which used brachytherapy-specific acquisition techniques such as modified reconstruction kernels and artifact-correction algorithms to reduce imaging artifacts. Axial CT scans with a slice thickness of 2 mm were obtained, completely covering the applicator and the surrounding phantom volume. The reconstructed Digital Imaging and Communications in Medicine (DICOM) dataset was then imported into the Oncentra Brachy treatment planning system (version 4.4, Elekta AB, Sweden) for dose computation and treatment planning.

## 2.3. Dose Distribution and Treatment Planning

The Oncentra TPS was used to prepare the irradiation plan. The program permitted precise contouring of the applicator, defining of the intrauterine channel, and identification of the exact path that the radioactive source would take. By calculating dwell periods at each place, the method guaranteed that the whole film wrapped around the applicator was evenly exposed to radiation. Because the applicator radius is constant in all directions, the centrally positioned source offered symmetric exposure, while the source's time-modulated stepping along the applicator axis ensured standardized and homogeneous dosage distribution across the whole film. The dwell sites were separated at 0.2 mm intervals along the applicator catheter.

As shown in Figure 3, the TPS interface displays both the optimization window, which shows normalized isodose distributions across the EBT3 film, and the 3D reconstruction of the applicator, which includes the source's intrauterine channel. Applicator reconstruction was carried out by contouring the applicator slice by slice on CT scans to ensure proper source channel localization. The software's tools enabled accurate catheter path identification, automated interpolation between slices, and complete 3D imaging of the applicator and surrounding phantom structures.



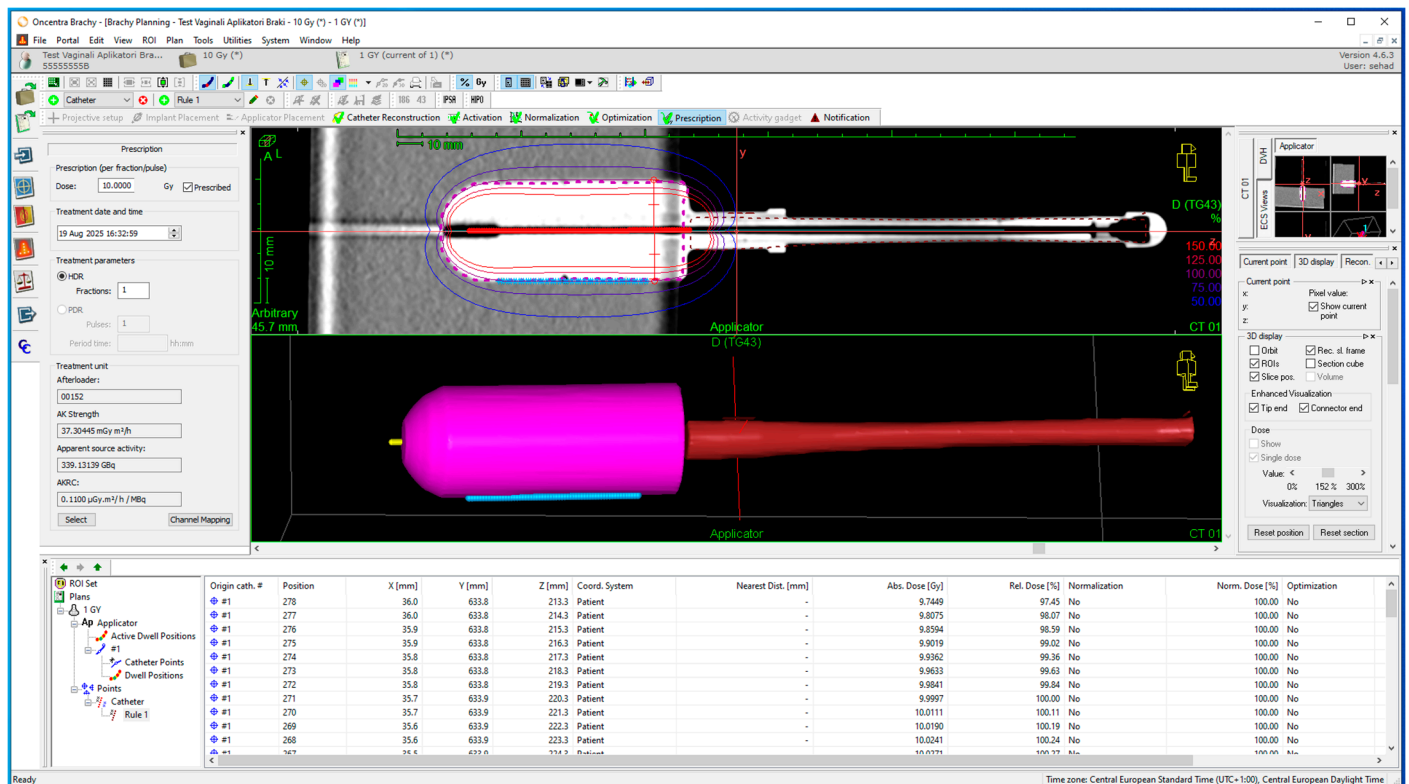


**Figure 3.** Treatment plan prepared in Oncentra TPS for 10 Gy at EBT3 film. The figure consists of two main panels accompanied by the technical data of the treatment plan. The upper panel displays the scanned applicator along with the corresponding dose distribution around it, while the lower panel presents the three-dimensional reconstructed applicator after contouring.

Reference points of interest were placed at a radial distance of 20.5 mm from the applicator center, at the same place where the radiochromic films were during radiation. Normalization was done separately for each calibration dose for six films for nominal doses of 0, 0.5, 1.0, 3.0, 7.0, and 10.0 Gy. Optimization algorithms were then used to homogenize the dosage distribution throughout the applicator surface while retaining clinically appropriate dwell time modulation. The design generated included precise information for each dwell location, as well as absolute and relative doses for each point.

#### 2.4. Irradiation Procedure

The radioactive Ir-192 source was delivered through the applicator's intrauterine channel and connected directly to the HDR afterloader (Flexitron, Elekta AB, Stockholm, Sweden) via a transfer tube. This system enabled the automated transfer of the source from the afterloader to the applicator, resulting in consistent and clinically correct irradiation. The source dwell positions and dwell lengths were rigorously established based on the treatment plan generated in Oncentra Brachy, allowing for perfect control over the exposure supplied to each film. As a result, the absorbed dose recorded by the film was controlled by the planned dwell time and current source activity, which accurately replicated clinical HDR brachytherapy circumstances.

To ensure consistency between treatment planning and actual delivery, the applicator was irradiated in the same water phantom used in the CT simulation under identical geometric and dosimetric conditions. Each calibration film was irradiated at a specific nominal dose (0, 0.5, 1.0, 3.0, 7.0, or 10.0 Gy) and analyzed separately, with its optical density values normalized to the corresponding planned dose from the TPS. This procedure ensured that the calibration curve was built on consistent reference points across all six

films. To assure procedural accuracy, the Flexitron afterloader's internal quality assurance system monitored source step accuracy, dwell duration precision, and emergency retraction capabilities throughout the irradiation process. Figure 4 shows the film dosimeters' irradiation setup, indicating how the nominal doses were administered in accordance with the treatment plan.



**Figure 4.** The HDD Flexitron afterloader and applicator with wrapped EBT3 in water phantom during irradiation.

The radioactive source employed was Iridium-192 (Ir-192), which was enclosed in a stainless steel capsule with a typical active core length of 3.5–5 mm and a diameter of 0.6–0.9 mm, and sealed within a welded capsule of around 4.5 mm overall length. This compact design enables consistent transit through applicators as tiny as 6F while preserving structural integrity and radiation safety. At installation, the source exhibited an activity of 468.6 GBq (~12.7 Ci), which is comparable with the initial loading for clinical HDR brachytherapy. Considering the physical half-life of 73.83 days, the activity drops by about 1% per day. At the time of this research, the source had declined to 201.6 GBq (~5.45 Ci), which was sufficient for clinical treatment and experimental dosimetric validation. Ir-192 decays by  $\beta$ -emission with a complicated  $\gamma$ -ray spectrum. Photon energies range from 136 keV to 1064 keV, with an average emission energy of roughly 380 keV. This provides an effective balance of penetration and localized dose deposition in tissue-equivalent media.

According to the International Atomic Energy Agency (IAEA), HDR Ir-192 sources are classified as Category 2 sealed sources [15], which can inflict permanent damage or major health effects after short-term, uncontrolled exposure. To ensure radiation protection and source security, all irradiation treatments were carried out in a shielded treatment bunker built to international radiological safety standards. The bunker has thick, high-density concrete walls, automatic door interlocks, continuous area radiation monitoring,

and emergency source retraction mechanisms integrated with the afterloader. These safety procedures ensure controlled therapeutic dose administration while reducing radiation risks to staff and guaranteeing safe handling of the high-activity radioactive source.

### 2.5. Scanning the Irradiated EBT3 Films

After irradiation, all films were stored in light-protected envelopes and scanned 24 h later to ensure that the polymerization process was stable, reducing temporal changes in optical density. Scanning was carried out using an Epson Expression 12000XL flatbed scanner (Epson America Inc., Los Alamitos, CA, USA) in transmission mode, with the Transparency Unit as the document source. Prior to scanning, the device was permitted to run a typical warm-up routine to stabilize the light source output, as per established dosimetric guidelines.

The scanner was set to Photo Mode, with 48-bit color depth and 150 dpi resolution, and photos were saved in uncompressed TIFF format to preserve the entire dynamic range of the pixel values. To increase dose–response repeatability, only the red channel was investigated because it had the highest sensitivity for EBT3 films within the absorbed dose range of 0–10 Gy. To prevent post-processing artifacts, all image correction and enhancement capabilities were disabled, including automated exposure, sharpening, and color management. This technique is consistent with prior research recommendations, which emphasize the need to retain raw picture integrity for correct optical density versus dosage calibrations.

Furthermore, films were regularly put in the scanner's middle region to reduce lateral response artifacts, as differences in scanner light uniformity throughout the scanning bed can cause systematic mistakes. Each film was scanned in the same orientation, as orientation-dependent effects have been recorded due to the scanner light source's anisotropic reaction to the film's polymer structure. These techniques improved the reliability of the digitization process and reduced uncertainty in later dosimetric analysis.

### 2.6. Calibration Curve

To create the calibration curve, the net optical density (NOD) of irradiated Gafchromic EBT3 sheets was compared to the given dose. The connection between dosage and NOD is essentially nonlinear, as polymerization in the active layer grows in a saturation-like manner with increasing radiation. As a result, empirical fitting functions such as polynomial, exponential, and rational models are often used, and they have been extensively validated in the literature for the 0–10 Gy range that is typical of HDR brachytherapy dosimetry. The general form of the calibration function converts measured pixel values to absorbed dose, allowing for quantitative dose mapping.

In radiochromic film dosimetry, the use of net optical density (NOD) is preferred because it introduces an additional correction that eliminates background effects and inhomogeneities across the film. NOD is defined as:

$$NOD = \log_{10} \left( \frac{I_{unexp}}{I_{exp}} \right) - \log_{10} \left( \frac{I_{unexp}}{I_{ref}} \right) \quad (1)$$

where

$I_{unexp}$  is the mean pixel value of the unexposed film (background);

$I_{exp}$  is the mean pixel value of the irradiated film region;

$I_{ref}$  is the mean pixel value of a reference region of interest (ROI) in the same film sheet that has not received a dose.

This simplification assumes that the background reference  $I_{unexp}$  and the unexposed control  $I_{unexp}$  are equivalent, which is valid when all calibration films are cut from the same



sheet and scanned under identical conditions. By applying NOD rather than OD alone, the calibration curve reflects only radiation-induced changes in film darkening, thereby improving reproducibility and accuracy in dose–response measurements for HDR brachytherapy.

After the experiment was conducted, several functional forms were tested, including second-order polynomial (Equation (2)) [10,16,17] and rational function (Equation (3)) recommended by producer. The experimental results, however, agreed best with the second-order polynomial function, which was presented in Equation (2):

$$D = a \times NOD^2 + b \times NOD + c \quad (2)$$

where  $a$  is the quadratic coefficient,  $b$  is linear coefficient, and  $c$  is the intercept.

$$D = d + \frac{e}{(NOD - f)} \quad (3)$$

where  $d$  is for horizontal asymptote,  $e$  scale factor and  $f$  the vertical asymptote.

## 2.7. Manual and Automatic ROI Selection

A unique MATLAB (R2024b) tool was written to systematically compare manual and automated ROI selection procedures in film calibration. The manual approach involves the operator interactively defining rectangular regions of interest (ROIs) on each scanned film image. For this investigation, five ROIs were chosen per film to ensure that repeated measurements might be statistically comparable. Each ROI was created using the MATLAB graphical interface, with the operator purposely including areas that could have film flaws, scanner non-uniformities, or handling artifacts. This is consistent with the traditional approach employed in most published calibration workflows, in which the investigator uses visual inspection to determine representative sections of the film. Because the operator can select different locations in each replicate, manual selection is fundamentally subjective and susceptible to operator experience, intuition, and even prejudice. Nonetheless, this flexibility enables an expert to focus on areas that appear to be most indicative of the global film response, which can occasionally result in improved dose–response alignment even when local artifacts are present.

In contrast, the automatic system conducts an objective statistical search across the whole usable film area. First, border pixels and areas suspected of having text labels or scanner glare are excluded. Within the remaining “core” film mask, the algorithm constructs a dense grid of candidate rectangles of varied sizes and aspect ratios (20–30% of the film dimensions, width-to-height ratios of 1.0, 1.5, and 0.67). The weighted evaluation function combined two criteria: the internal homogeneity of pixel values (low standard deviation) and the proximity of the median intensity of the candidate ROI to the global film median. This combination was chosen to minimize the impact of local artifacts or scanner non-uniformities, while maintaining consistency across the film. Sensitivity tests showed that moderate variations in the weighting scheme did not significantly change the calibration curve within the studied dose range, confirming the robustness of the approach. A weighted scoring function combines these variables, and the ROI with the lowest score is chosen as ideal.

To simulate replicate measurements, the operation is carried out five times for each film. Following the initial ROI selection, subsequent selections are punished if they overlap with previously selected ROIs (via an intersection-over-union, IoU, penalty). This guarantees that the five automatically determined ROIs are spread out across the film rather than concentrated in a single uniform zone. As a result, the automated technique captures several representative areas while avoiding regions of high variance or artifacts.

Both methods generate five replicate measurements of net optical density (NoD) per film, but through fundamentally different mechanisms: the manual approach relies on the operator's judgment in drawing ROIs, whereas the automatic algorithm searches the image systematically to find homogeneous zones that statistically resemble the overall film response. The ROI dimensions (about 20–30% of the image width and height) are large enough to produce a consistent pixel population while remaining small enough to sample multiple subregions of the film.

This dual technique allows for a direct comparison between operator-dependent and algorithm-driven calibration. The manual method frequently catches the overall film reaction, albeit with greater variability among repeats, whereas the automatic method ensures reproducibility and homogeneity at the expense of potential bias if systematic scanner effects are present. In both procedures, net optical density (NOD) data are retrieved, and second-order polynomial functions are used to construct calibration curves. Statistical criteria like  $R^2$ , RMSE, and MAE evaluate curve quality objectively.

The primary purpose of this implementation is not just to reduce operator dependency but also to test whether automated ROI selection has measurable advantages over standard human ROI selection. This study examines two methodologies using identical film files to see which yields more stable and consistent calibration for clinical brachytherapy dosimetry.

## 2.8. Visualizations of Film Dose

The second MATLAB algorithm was written to convert scanned film pictures into quantifiable 2D and 3D dosage maps based on the calibration curve obtained from EBT3 films. Every pixel was converted to absorbed dosage (Gy) based on the calibration curve. To reduce the noise, the code applies a robust median filter to the NOD map prior to dosage conversion. A film/background segmentation stage generates a binary mask to evaluate only pixels from the film.

For 2D dose images, the software creates a false-color dose map with six discrete bands whose interval boundaries are adaptively defined by the film's dose distribution. This dynamic binning increases contrast across different exposures and standardizes color bar labels to certain Gy ranges. The operator can examine isodose structure, hotspot/coldspot patterns, and band occupancy directly on the film plane, with no geometric mirroring relative to the scanner coordinate system.

The program provides a 3D representation, with the x-y axes representing film coordinates (pixels or mm after selectable scaling) and the z axis representing absorbed dose. To ensure visual consistency, the 3D surface uses the same color scale as the 2D map, and interactive controls allow for quick changes in viewpoint and axis direction. In addition to full-field rendering, the interface allows you to limit the visualization to an operator-defined subregion of interest (ROI). The selected zone is subsequently rendered in 3D, allowing for precise inspection of local heterogeneities, seam artifacts, or applicator-proximal regions without interference from the remainder of the film.

The program provides a 3D representation, with the x-y axes representing film coordinates (pixels or mm after selectable scaling) and the z-axis representing absorbed dose. To ensure visual consistency, the 3D surface uses the same color scale as the 2D map, and interactive controls allow for quick changes in viewpoint and axis direction. In addition to full-field rendering, the interface allows you to limit the visualization to an operator-defined subregion of interest (ROI). The selected zone is subsequently rendered in 3D, allowing for precise inspection of local heterogeneities, seam artifacts, or applicator-proximal regions without interference from the remainder of the film.

### 3. Results and Discussion

#### 3.1. Calibration Curves with Automatic Versus Manual ROI

After finishing the computing procedure for five irradiated films, five manual and five automatic ROI selections were performed, yielding data in Table 1, which illustrates the comparative results between them.

**Table 1.** Comparative table between manual and auto ROI selection; each film was selected 5 times.

Nr.	Nominal Dose (Gy)	Manual		Automatic	
		Mean	Standard Deviation	Mean	Standard Deviation
1	0.0	−0.008	0.003	0.000	0.001
2	0.5	0.042	0.009	0.021	0.001
3	3.0	0.112	0.006	0.136	0.005
4	7.0	0.316	0.005	0.304	0.001
5	10.0	0.381	0.004	0.389	0.003

The validity of the method was confirmed by comparing the calibration results with the reference dose values from the TPS, while reproducibility and repeatability were assessed by analyzing five independent ROIs per film and repeating the measurements across six irradiated films. The normalization was incorporated into the automatic ROI selection, which increased the stability of the calibration results. Using robust z-score normalization during automatic processing reduced variability across replicates, resulting in lower RMSE and MAE values when compared to the non-normalized technique. This demonstrates that normalization improves the robustness and consistency of automatic calibration, making the findings less prone to image noise and background artifacts.

At the 0 Gy reference level, both techniques generate unstable findings, as expected given the low optical density signal and sensitivity to background noise. The coefficient of variation (CoV) for the manual method is particularly high because the denominator (mean NoD) approaches zero.

At 0.5 Gy, the manual method produces a higher mean NoD (0.042) than the automatic method (0.021). Both methods have low standard deviation. This suggests that at low doses, manual ROI selection may provide a slightly stronger dose–response signal, but both methods are reproducible.

At the intermediate dose of 3 Gy, the manual technique gives a lower result than the automatic option NoD (0.112 vs. 0.136), with respective standard deviation values 0.006 and 0.005. The automatic technique shows lower variability, indicating greater stability at this dose level. This emphasizes an important distinction: the automated approach is less subject to fluctuation, but its dose–response slope may be overestimated when compared to manual selection.

At 7 Gy, the manual had a larger mean than automatic approach NoD (0.316 vs. 0.304) and standard deviation 0.005 and 0.001. The automatic approach is quite consistent in this case, but the shift in mean NoD shows a systematic bias that must be considered when evaluating calibration results.

Finally, at the greatest dose (10 Gy), the automatic method produces the strongest dose–response signal, with a mean NoD of 0.389, whereas the manual method understates the response (0.381). The negative coefficient on manual selection for film dose 0.0 Gy is caused by operator-dependent biases and the presence of nonuniform regions; it indicates unrealistic behavior at low doses, confirming the limitations of the manual ROI approach. In the automatic model, there is no negative value.

Four dose–response calibration curves were performed based on Table 1 data, with NOD as the predictor and a second-order polynomial model and rational model as the response function. The resulting calibration curves are depicted in Figure 5a (Manual ROI) and Figure 5b (Auto ROI). Fits are visualized only inside the measured NOD domain, without any extrapolation.

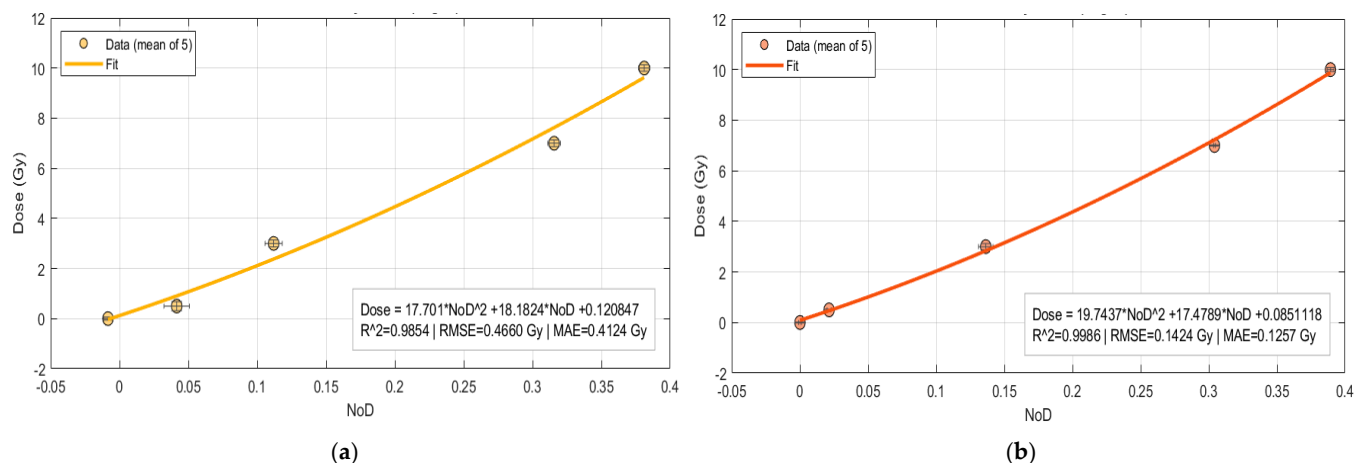


**Figure 5.** Calibration curve of film dosimetry for polynomial model: (a) Manual ROI and (b) Automatic ROI.

The comparison between manual and automatic ROI calibration models for second polynomial model shows considerable disparities in statistical performance. The automatic ROI approach produced a quadratic fit as presented in Equation (4), with a good coefficient of determination  $R^2 = 0.998$ . The related error measures were minimal, with a Root Mean Square Error (RMSE) of 0.142 Gy and a Mean Absolute Error (MAE) of 0.126 Gy. These results show that the automated approach accurately captures the film’s dose–response relationship, resulting in a smooth calibration curve that closely reflects the experimental data across the whole dose range.

$$D = 19.74NOD^2 + 17.7NOD + 0.08 \quad (4)$$

In contrast, the manual ROI approach gave a function fit as presented in Equation (5), with a lower coefficient of determination  $R^2 = 0.985$ . The error statistics were significantly greater, with an RMSE of 0.466 Gy and an MAE of 0.413 Gy. These findings represent increased variability and scatter in the manually selected ROIs, especially at higher treatment levels where departures from the targeted dose became more noticeable. The negative coefficient on the quadratic term also indicates a concave curvature not seen in the automated model, which is most likely due to operator-dependent biases and the presence of nonuniform regions; it indicates unrealistic behavior at low doses, confirming the limitations of the manual ROI approach.

$$D = 17.7NOD^2 + 18.18NOD + 0.12 \quad (5)$$

The results for rational models for both manual and automatic are shown in

The manual ROI approach for rational model is presented in Equation (6), with a coefficient of determination  $R^2 = 0.986$  and with statistical parameters RMSE of 0.448 Gy and an MAE of 0.388 Gy.

$$D = \frac{73,854.3NOD + 781.99}{-3573.3NOD + 4334.9} \quad (6)$$

On the other hand, the automatic ROI approach for rational model fit as presented in Equation (7), with a very good coefficient of determination  $R^2 = 0.999$  and with RMSE of 0.118 Gy and a MAE of 0.103 Gy.

$$D = \frac{8.94NOD + 0.043}{-0.357NOD + 0.494} \quad (7)$$

The comparative analysis of polynomial 2nd degree and rational models reveals that automatic ROI selection outperforms manual ROI selection. The automatic example regularly shows greater coefficients of determination  $R^2$ , and lower RMSE and MAE values. Figure 6.

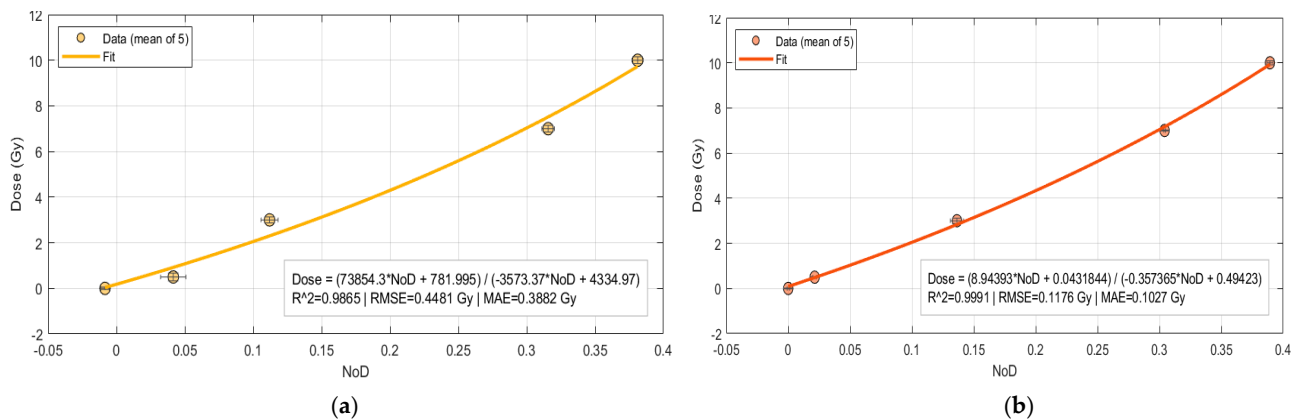


**Figure 6.** Calibration curve of film dosimetry for rational model: (a) Manual ROI and (b) Automatic ROI.

When comparing the models, the rational function outperforms the quadratic polynomial in terms of overall fit, regardless of whether the ROI is selected manually or automatically. This shows that the rational model is better suited to describing the nonlinear dose–response behavior of EBT3 films.

It is also worth noting that the automatic approach not only lowers user dependency and inter-observer variability, but it also improves the calibration process’s reproducibility. Taken together, these findings show that the rational function combined with automatic ROI selection produces the most consistent and accurate calibration and hence can be suggested as the optimal method.

### 3.2. MATLAB-Based 3D Dose Reconstruction

To expand the use of the calibration curve, a custom MATLAB script was created to reconstruct two- and three-dimensional dose distributions from irradiated EBT3 films. The application reads the scanned film image (TIFF format), uses Figure 6b calibration curve to convert pixel intensity to absorbed dose, and outputs a 3D surface with the x-y axes representing physical film dimensions (mm) and the z-axis representing absorbed dosage (Gy).

The panels in Figure 7 show how the film signal progresses from the raw scan to calibrated 2D and 3D dose representations at two dose levels. The left column represents the film irradiated at 3 Gy, whereas the right column represents 10 Gy. The raw scans in the top row demonstrate the expected rise in optical density with dose: the 10 Gy film is significantly darker and more uniform in the core area, whereas the 3 Gy film seems lighter and more prone to minor shading and handling marks near the margins.



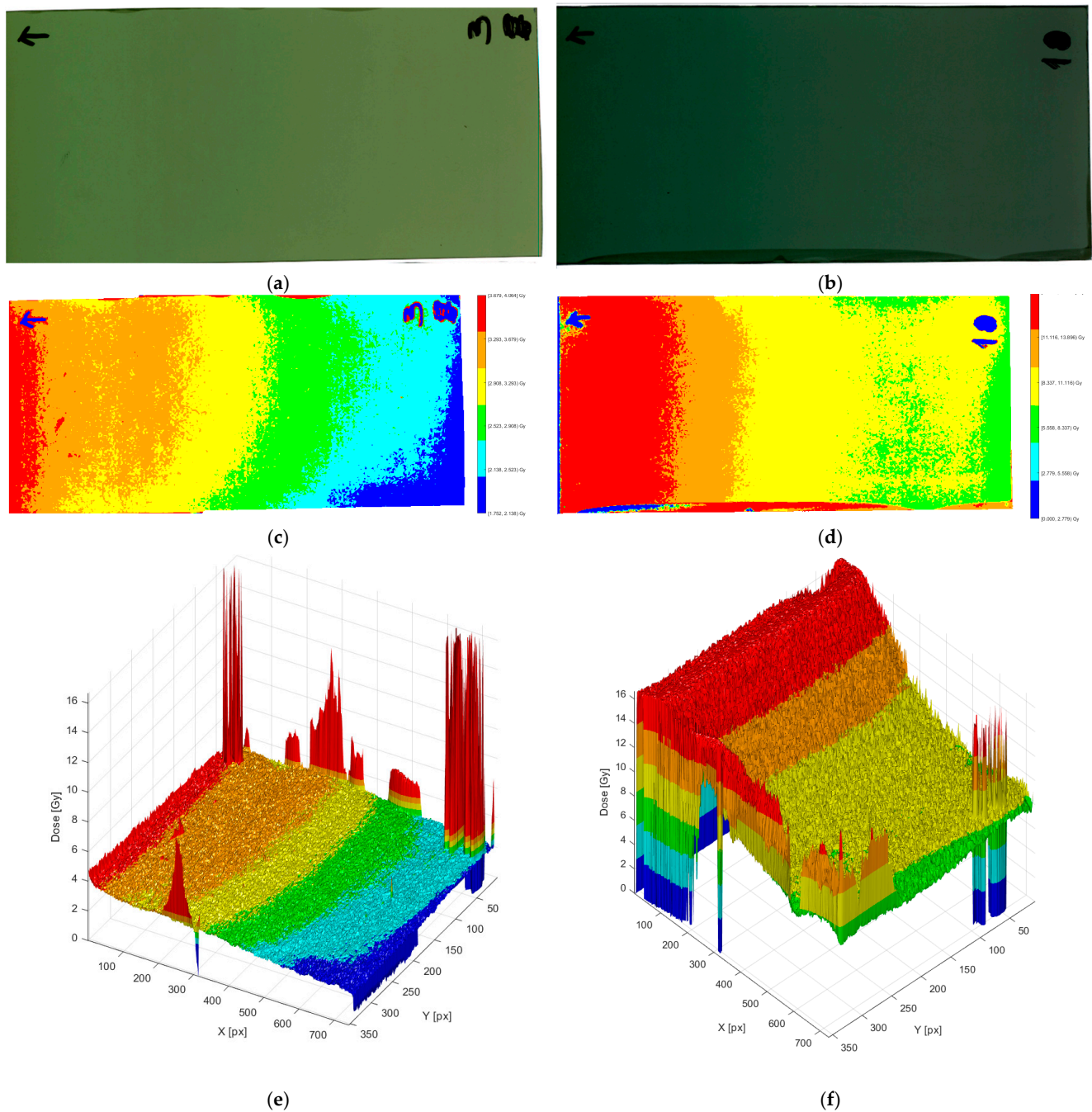


**Figure 7.** Irradiated EBT3 Film and Their Dose Visualization. The subfigures (a,b) also include the arrow indicating the film orientation and the number used for identification. The colors in subfigures (c–f) represent the dose distribution in Gray (Gy), with red indicating the highest dose and blue corresponding to the lowest dose: (a) Scanned film irradiated with 3 Gy, (b) Scanned film after irradiated with 10 Gy, (c) Visualizations of 2D absorbed dose with 3 Gy, (d) Visualizations of 2D absorbed dose with 10 Gy, (e) Visualizations of 3D absorbed dose for 3 Gy, (f) Visualizations of 3D absorbed dose for 10 Gy.

Following the calibration curve, the center row transforms the photos into false color 2D dosage maps with six adaptive bands. At 3 Gy, the map has a greater range of intermediate bands and a moderate lateral gradient, indicating a reduced signal-to-noise ratio at a modest dose. At 10 Gy, higher-dose bands dominate, and the middle field appears smoother, indicating increased SNR and dose distribution. Small localized “hot” or “cold” patches along edges and annotations are apparent in both scenarios; they are removed

from quantitative ROI analysis since they are caused by scanner glare/labels rather than dosimetry effects. These edge pieces must be avoided in both automatic ROI selection and manual selection since they will have a detrimental impact on the calibration dose.

The bottom row shows 3D dosage surfaces, with the z-axis representing absorbed dose (Gy). The 3 Gy surface has a lower-amplitude relief with many small spikes aligned with non-dosimetric markers; other than these, the surface is rather smooth, indicating good homogeneity for this exposure. The 10 Gy surface rises to a higher, flatter plateau with better band transitions and fewer small-scale oscillations, which is consistent with the film readout's superior precision at larger doses. Overall, Figure 5 shows that calibrated film analysis captures the global dose gradient and local inhomogeneities in a visually intuitive (2D bands) and metrically informative (3D relief) manner, thereby supporting subsequent heterogeneity metrics and qualitative trends reported elsewhere in the results.

This 3D technique has the advantage of converting point- or line-based film dosimetry measurements into full-field dose deposition maps. This visualization improves the detection of potential inhomogeneities, such as isolated hot patches or cold regions, and is a dependable recording tool for clinical quality control. Furthermore, the software-based approach allows for the direct integration of film dosimetry into conventional QA procedures, resulting in both qualitative and quantitative assessments of applicator performance.

While intraday reproducibility was assessed through multiple ROI extractions within the same irradiation and scanning session, interday reproducibility was not explicitly evaluated in this study. Future work will include repeated irradiation and scans on different days to further validate the long-term stability and robustness of the proposed methodology.

#### 4. Conclusions

This work shows that automatic ROI selection has significant advantages over human ROI definition for film calibration. The automatic method not only improves calibration accuracy, but it also lowers operator dependence and increases repeatability across repetitions. The integration of normalization within the automatic workflow is a significant methodological improvement. Normalization improves the calibration process by normalizing image distributions during ROI recognition, reducing the influence of background noise or artifacts.

In terms of mathematical models, both second-order polynomials and rational functions were examined. While both models accurately represent the dose–response relationship, the rational function consistently outperformed the polynomial in terms of fit quality, regardless of ROI type. The most accurate and reliable calibration approach is thus achieved by combining rational modeling with automatic ROI selection and normalization.

The innovative contribution of this study lies in the combination of automated ROI selection and MATLAB-based 2D/3D dose reconstruction, creating a novel and integrated workflow for HDR brachytherapy film dosimetry. This approach reduces operator dependency, enhances reproducibility, and offers a comprehensive tool for routine clinical quality assurance.

**Author Contributions:** Conceptualization, G.H.; Data curation, L.K.; Formal analysis, G.H. and S.K.; Investigation, B.U. and P.D.; Methodology, B.R.; Project administration, K.G.; Software, G.H. and F.S.; Supervision, L.K.; Validation, H.S.; Visualization, S.K.; Writing—original draft, G.H. and L.K.; Writing—review and editing, B.U. and S.K. All authors have read and agreed to the published version of the manuscript.

**Funding:** This research has been partially supported by “AL TRADE CENTER” LLC, St “Mother Teresa”, 12 000, Fushë Kosovë, Kosovë.

**Institutional Review Board Statement:** Not applicable.

**Informed Consent Statement:** Not applicable.

**Data Availability Statement:** The data presented in this study are available from the corresponding author upon reasonable request.

**Acknowledgments:** During the preparation of this manuscript, the authors partially used ChatGPT 4.5 as a text generator. The authors have reviewed and edited the output and take full responsibility for the content of this publication.

**Conflicts of Interest:** The authors declare no conflicts of interest.

## Abbreviations

The following abbreviations are used in this manuscript:

HDR	High Dose Rate
EBT3	Gafchromic EBT3
ROI	Region of Interest
OD	Optical Density
NOD	Net Optical Density
QA	Quality Assurance
Gy	Gray
Ir-192	Iridium-192
Co-60	Cobalt-60
CT	Computed Tomography
MR	Magnetic Resonance
TIFF	Tagged Image File Format
dpi	dots per inch
2D	Two-Dimensional
3D	Three-Dimensional
TPS	Treatment Planning System
DICOM	Digital Imaging and Communications in Medicine
RMSE	Root Mean Square Error
MAE	Mean Absolute Error

## References

1. Pathak, P.; Thomas, J.J.; Baghwala, A.; Li, C.; Teh, B.S.; Butler, E.B.; Farach, A.M. Personalized Brachytherapy: Applications and Future Directions. *Cancers* **2024**, *16*, 3424. [[CrossRef](#)] [[PubMed](#)]
2. Skowronek, J. Current status of brachytherapy in cancer treatment—Short overview. *J. Contemp. Brachyther.* **2017**, *9*, 581–589. [[CrossRef](#)] [[PubMed](#)]
3. Kastrati, L.; Hodolli, G.; Kadiri, S.; Demirel, E.; Istrefi, L.; Kabashi, Y.; Uka, B. Applications and benefits of using gradient percentage depth dose instead of percentage depth dose for electron and photon beams in radiotherapy. *Pol. J. Med. Phys. Eng.* **2021**, *27*, 25–29. [[CrossRef](#)]
4. Doudoo, C.O.; Gyekye, P.K.; Emi-Reynolds, G.; Kpeglo, D.O. A comparative study between MC simulation and TLD measurements of radiation doses to other parts of the body during gynaecological brachytherapy. *Health Technol.* **2024**, *14*, 1113–1121. [[CrossRef](#)]
5. Lopes, A.; Sabondjian, E.; Baltazar, A.R. In Vivo Dosimetry for Superficial High Dose Rate Brachytherapy with Optically Stimulated Luminescence Dosimeters: A Comparison Study with Metal-Oxide-Semiconductor Field-Effect Transistors. *Radiation* **2022**, *2*, 338–356. [[CrossRef](#)]
6. Yoosuf, A.B.M.; Jeevanandam, P.; Whitten, G.; Workman, G.; McGarry, C.K. Verification of high-dose-rate brachytherapy treatment planning dose distribution using liquid-filled ionization chamber array. *J. Contemp. Brachyther.* **2018**, *10*, 142–154. [[CrossRef](#)] [[PubMed](#)]
7. Asgharizadeh, S.; Bekerat, H.; Syme, A.; Aldelaijan, S.; DeBlois, F.; Vuong, T.; Evans, M.; Seuntjens, J.; Devic, S. Radiochromic film-based quality assurance for CT-based high-dose-rate brachytherapy. *Brachytherapy* **2015**, *14*, 578–585. [[CrossRef](#)] [[PubMed](#)]
8. Oustous, A.; Airouss, Z.; Attaoui, Y.E.; Oustous, Y.; Khalis, M.; Sebihi, R. Dosimetry evaluation of 192Ir Flexisource using gafchromic EBT3 film. *J. Radiother. Pract.* **2024**, *23*, e24. [[CrossRef](#)]

9. Ayoobian, N.; Asl, A.S.; Poorbaygi, H.; Javanshir, M.R. Gafchromic film dosimetry of a new HDR brachytherapy source. *J. Appl. Clin. Med. Phys.* **2016**, *17*, 194–205. [[CrossRef](#)] [[PubMed](#)]
10. Huang, L.; Gaballa, H.; Chang, J. Evaluating dosimetric accuracy of the 6 MV calibration on EBT3 film in the use of Ir-192 high dose rate brachytherapy. *J. Appl. Clin. Med. Phys.* **2022**, *23*, e13571. [[CrossRef](#)] [[PubMed](#)]
11. Salamat, F.; Siavashpour, Z.; Sadeghi, M.; Jaber, R.; Gholami, S. Dosimetric evaluation and Monte Carlo simulation of a new proposed surface brachytherapy mould. *J. Contemp. Brachyther.* **2024**, *16*, 279–288. [[CrossRef](#)] [[PubMed](#)]
12. Oliver-Cañamás, L.; Rovira-Escutia, J.J.; Vijande, J.; Candela-Juan, C.; Gimeno-Olmos, J.; Pujades-Claumarchirant, M.C.; Martínez-Navarro, J.Á.; Zaragoza-Carrillo, A.; García-Cases, F.; Ballester, F.; et al. A system for mailed dosimetric audits of <sup>192</sup>Ir and <sup>60</sup>Co HDR brachytherapy combining OSLD and radiochromic film. *Radiat. Meas.* **2024**, *173*, 107101. [[CrossRef](#)]
13. McNairn, C.; Mansour, I.; Muir, B.; Thomson, R.M.; Murugkar, S. High spatial resolution dosimetry with uncertainty analysis using Raman micro-spectroscopy readout of radiochromic films. *Med. Phys.* **2021**, *48*, 4610–4620. [[CrossRef](#)] [[PubMed](#)]
14. Rieker, V.F.; Bateman, J.J.; Wroe, L.M.; Caloz, M.; Grilj, V.; Aguiar, Y.Q.; Schüller, A.; Bailat, C.; Farabolini, W.; Gilardi, A.; et al. Radiochromic Film Dosimetry for VHEE and UHDR: Considerations for the CLEAR Facility and Comparisons with Alanine, RPL and Dosimetry Phantoms. *arXiv* **2025**, arXiv:2506.16837. [[CrossRef](#)]
15. Verma, R.; Jain, G.K.; Chougule, A. Implementation of safety and security standards for high dose rate brachytherapy sealed radioactive source used in a medical radiation facility. *Radiat. Med. Prot.* **2020**, *1*, 166–170. [[CrossRef](#)]
16. Chang, L.; Yeh, S.-A.; Ho, S.-Y.; Ding, H.-J.; Chen, P.-Y.; Lee, T.-F. Calibration of the EBT3 Gafchromic Film Using HNN Deep Learning. *Biomed Res. Int.* **2021**, *2021*, 8838401. [[CrossRef](#)] [[PubMed](#)]
17. Vadrucci, M.; Esposito, G.; Ronsivalle, C.; Cherubini, R.; Marracino, F.; Montereali, R.M.; Picardi, L.; Piccinini, M.; Pimpinella, M.; Vincenti, M.A.; et al. Calibration of GafChromic EBT3 for absorbed dose measurements in 5 MeV proton beam and (<sup>60</sup>Co)  $\gamma$ -rays. *Med. Phys.* **2015**, *42*, 4678–4684. [[CrossRef](#)] [[PubMed](#)]

**Disclaimer/Publisher’s Note:** The statements, opinions and data contained in all publications are solely those of the individual author(s) and contributor(s) and not of MDPI and/or the editor(s). MDPI and/or the editor(s) disclaim responsibility for any injury to people or property resulting from any ideas, methods, instructions or products referred to in the content.